Erschienen in: Nature Nanotechnology ; 14 (2019), 7. - S. 658-661
https://dx.doi.org/10.1038/s41565-019-0436-8

Thermal skyrmion diffusion used in a reshuffler device

Jakub Zázvorka[1,2], Florian Jakobs[3], Daniel Heinze[1], Niklas Keil[1], Sascha Kromin[1], Samridh Jaiswal[1,4], Kai Litzius[1,5,6], Gerhard Jakob[1,5], Peter Virnau[1], Daniele Pinna[1], Karin Everschor-Sitte[1,5], Levente Rózsa[7], Andreas Donges[3], Ulrich Nowak[3] and Mathias Kläui[1,5]*

Magnetic skyrmions in thin films can be efficiently displaced with high speed by using spin-transfer torques[1,2] and spin–orbit torques[3–5] at low current densities. Although this favourable combination of properties has raised expectations for using skyrmions in devices[6,7], only a few publications have studied the thermal effects on the skyrmion dynamics[8–10]. However, thermally induced skyrmion dynamics can be used for applications[11] such as unconventional computing approaches[12], as they have been predicted to be useful for probabilistic computing devices[13]. In our work, we uncover thermal diffusive skyrmion dynamics by a combined experimental and numerical study. We probed the dynamics of magnetic skyrmions in a specially tailored low-pinning multilayer material. The observed thermally excited skyrmion motion dominates the dynamics. Analysing the diffusion as a function of temperature, we found an exponential dependence, which we confirmed by means of numerical simulations. The diffusion of skyrmions was further used in a signal reshuffling device as part of a skyrmion-based probabilistic computing architecture. Owing to its inherent two-dimensional texture, the observation of a diffusive motion of skyrmions in thin-film systems may also yield insights in soft-matter-like characteristics (for example, studies of fluctuation theorems, thermally induced roughening and so on), which thus makes it highly desirable to realize and study thermal effects in experimentally accessible skyrmion systems.

We investigated skyrmions in specially developed low-pinning Ta(5)/$Co_{20}Fe_{60}B_{20}$(1)/Ta(0.08)/MgO(2)/Ta(5) (nanometre thickness of the layers shown in parenthesis) stacks using magneto-optical Kerr effect (MOKE) microscopy (details given in Methods). By varying the out-of-plane field, we tailored the skyrmion density and radius. We nucleated single skyrmions in a deterministic fashion using current injection (Supplementary Video 1), and thereby controlled the density of the skyrmions precisely to avoid skyrmion–skyrmion interactions[14].

After the desired number of skyrmions were injected into a microstructured film element, we observed the skyrmions in real time with the Kerr microscope without any further current injection or any other external stimulus. In contrast to previous reports and our previous results in different stacks[4,5], here we clearly observed skyrmion motion after the system had relaxed with no further aftereffect of the current pulse (Supplementary Video 2). At constant conditions, the skyrmions moved randomly throughout the sample. To evaluate the diffusive skyrmion motion, individual skyrmions were tracked (Supplementary Video 3) and an example of several typical skyrmion trajectories is shown in Fig. 1. Having established motion without any external excitations, the first step was to identify the origin of the dynamics. One possible origin is the presence of thermal effects that can lead to diffusion in regimes that range from sub- to superdiffusive[15] or to Brownian motion. The different regimes can be identified from the mean squared displacement (MSD) of the measured skyrmions. For diffusive motion assuming rigid particles with no correlations (from here on denoted as pure diffusion), the average MSD is proportional to time. We therefore plotted the MSD:

$$\mathrm{MSD} = \langle |\mathbf{R}_\nu(\mathbf{t}) - \mathbf{R}_\nu(\mathbf{0})|^2 \rangle = 2Dtd \qquad (1)$$

as a function of the time t elapsed and calculated the diffusion coefficient D. The parameter d denotes the dimension of the system and takes the value of $d=2$ for our measurement. $\mathbf{R}_\nu$ is the position of a given skyrmion. As the evaluation of diffusion assumes a random motion of particles, to obtain statistically sound values of the diffusion coefficient the MSD of many particles has to be averaged and the skyrmions have to be treated as a statistical ensemble. The resulting average MSD as a function of time at room temperature is shown in the inset in Fig. 1. We find a linear dependence, as in equation (1), and a linear fit of the evaluated data reveals the diffusion coefficient of the material stack to be $D = 0.27(20) \times 10^{-12}\,\mathrm{m^2\,s^{-1}}$ at a temperature $T = 296\,\mathrm{K}$. With the MSD being linearly proportional to time and the diffusion constant above, we conclude that skyrmions exhibit diffusive dynamics, which is relevant at room temperature on macroscopic timescales. To compare our results with theoretical predictions[16] (details in Supplementary Figs. 1–3), we note that the central quantities are the gyrocoupling G and the dissipative tensor element D_T. The latter depends on the profile of the skyrmion, which may change with its size[17]. We therefore determined values of D_T for our studied skyrmions via a numerical integration of a skyrmion that was calculated by micromagnetic simulations for the appropriate material parameters of the experimentally used system. Surprisingly, our experimentally observed diffusion coefficient at room temperature was several orders of magnitude smaller than that predicted[16] for our experimental system ($D \cong 4 \times 10^{-8}\ \mathrm{m^2\ s^{-1}}$). However, even for the comparatively low diffusion coefficient values, we observed skyrmion displacement at a timescale of seconds. Hence, in addition to current-induced torques that can generate

[1]Institut für Physik, Johannes Gutenberg-Universität Mainz, Mainz, Germany. [2]Institute of Physics, Faculty of Mathematics and Physics, Charles University, Prague, Czech Republic. [3]Fachbereich Physik, Universität Konstanz, Konstanz, Germany. [4]Singulus Technologies AG, Kahl, Germany. [5]Graduate School of Excellence Materials Science in Mainz, Mainz, Germany. [6]Max Planck Institute for Intelligent Systems, Stuttgart, Germany. [7]Fachbereich Physik, Universität Hamburg, Hamburg, Germany. *e-mail: klaeui@uni-mainz.de

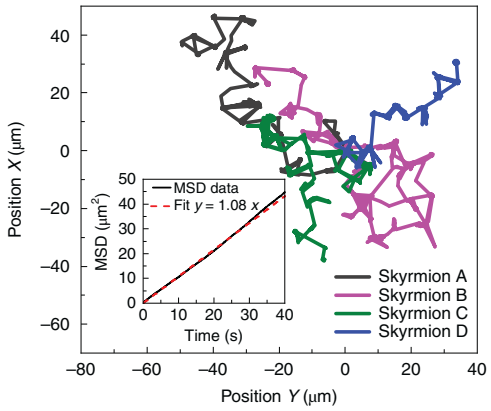

Fig. 1 | Trajectories of selected skyrmions at 296 K. The reference position was taken from the first frame in the measurement. All the skyrmions are set to start at position (0,0). The timescale of the observation is in the range of seconds to minutes. The inset shows the time-averaged MSD (black line) and the linear fit of the data (red dashed line).

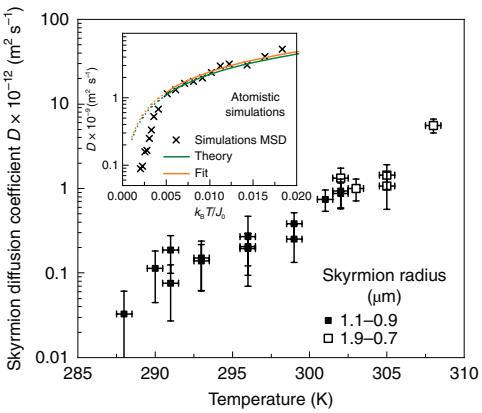

Fig. 2 | Temperature dependence of the evaluated skyrmion diffusion coefficient considering all the observed skyrmions. The linear dependence in the semilogarithmic plot shows a clear exponential dependence of the diffusion coefficient on temperature over two orders of magnitude. The error bars are calculated as the s.d. of the diffusion coefficient value over all measurements at a certain temperature. The inset shows the temperature dependence of the diffusion coefficient obtained from simulations (points) of a spin model with a non-flat energy potential landscape, normalized to the mean-field exchange constant $J_0 = 98$ meV (Supplementary Video 4). The simulation results likewise show a strongly enhanced temperature dependence at low temperature, which eventually transforms into the quasi-free diffusion expected from theory (line) at elevated temperatures.

skyrmion motion, thermal diffusion can also cause skyrmion dynamics and even be the dominant source of dynamics in a low-pinning system.

To understand this deviation of the diffusion coefficient from the prediction, we probed the diffusion behaviour of skyrmions as a function of temperature. We evaluated the MSD as a function of time for temperatures from 285 to 320 K. Pure diffusion behaviour holds for all the probed temperatures. The evaluated temperature dependence of the skyrmion diffusion coefficient is shown in Fig. 2, which reveals an exponential dependence.

Note that the measurement of the diffusion coefficient as a function of temperature includes a change of the skyrmion radius due to small changes in the magnetic properties with temperature. Although there is a small dependence of the skyrmion diffusion on radius (Supplementary Fig. 4), this cannot explain the observation that the diffusion coefficient depends exponentially on temperature (Fig. 2). Within the error bars, the temperature dependence can be described for the whole range, including the different skyrmion sizes, by a single exponential dependence, which shows that any effects of the size change have a negligible effect on the temperature dependence compared to the intrinsic thermal effect that leads to the exponential dependence. We concluded that the previously used assumption of rigid skyrmions in a translationally invariant environment[16,17] is not sufficient to describe our observations. To check the reason for this discrepancy, we further analysed the displacement from the experiment as a function of time and found that the skyrmions exhibited extended dwell times at certain positions (Supplementary Fig. 5). This means that we have to consider a non-flat potential landscape of the material on which skyrmions exhibit non-constant dwell times at certain positions due to the energy landscape that varies spatially. This process is, to some degree, analogous to the thermally activated movements of particles in solids[18].

To check if this explanation holds, we performed atomistic simulations using the well-studied model system[14] for a $Pt_{95}Ir_5$/Fe/Pd ultrathin film which, without any spatially varying energy landscape, confirms the previously published findings[16,17]. Given the spatial variations in the energy landscape, however, we reproduced the superlinear dependence of the diffusion coefficient for temperatures below the pinning energy barrier (Fig. 2 inset) and thus we obtained a qualitative agreement between simulations and experimental findings. At higher temperatures, the skyrmion motion becomes mostly unaffected by the pinning potential and we retain the theoretical solution for free skyrmion diffusion. This means that we can explain our experimental observations by simulations that consider a non-flat potential landscape. Reciprocally, we showed that the dwell times can be directly used to probe the potential landscape (Supplementary Fig. 5). In our simulations, the size changes of the skyrmions were not significant and the experimental behaviour was still reproduced, which shows that changes in the skyrmion size do not dominate the temperature dependence of the diffusion. If disorder becomes so sizeable that the skyrmion shape changes strongly (which we did not observe in the simulation, nor in the experiment), this will lead to possible additional effects that are beyond the scope of this work.

Beyond analysing the intrinsic system properties, thermal skyrmion dynamics has also been put forward as a mechanism that allows for signal decorrelation[13], a key missing component for probabilistic computing. Logic gates used in probabilistic computing circuits are very sensitive to correlations among input signals during operation. Correlated inputs result in unwanted propagations of correlations, which ultimately lead to incorrect computational results[13]. The latter has been predicted to be circumvented by a device denoted as a skyrmion reshuffler and it was theoretically shown that topologically non-trivial skyrmions are suitable spin structures that have an isotropic two-dimensional diffusion[13]. Suggestions to use skyrmions for token-based Brownian circuits were also studied recently[19].

For a proper operation, input signals have to be periodically reshuffled without altering the p value (signal up/down ratio) used in the actual computing step[20]. A first proof-of-concept can be performed by sampling telegraph noise signals and de-correlating them[13]. We sampled an input telegraph noise signal by generating a stream of skyrmions and successively scrambled it by driving the stream through a reshuffling chamber, which generated an output signal that was uncorrelated to the input while preserving p values with a high fidelity.

To implement the skyrmion reshuffler operation, we compared independent measurements for the respective 0-bit and 1-bit channels, as shown in Fig. 3. To evaluate the operation, we generated two

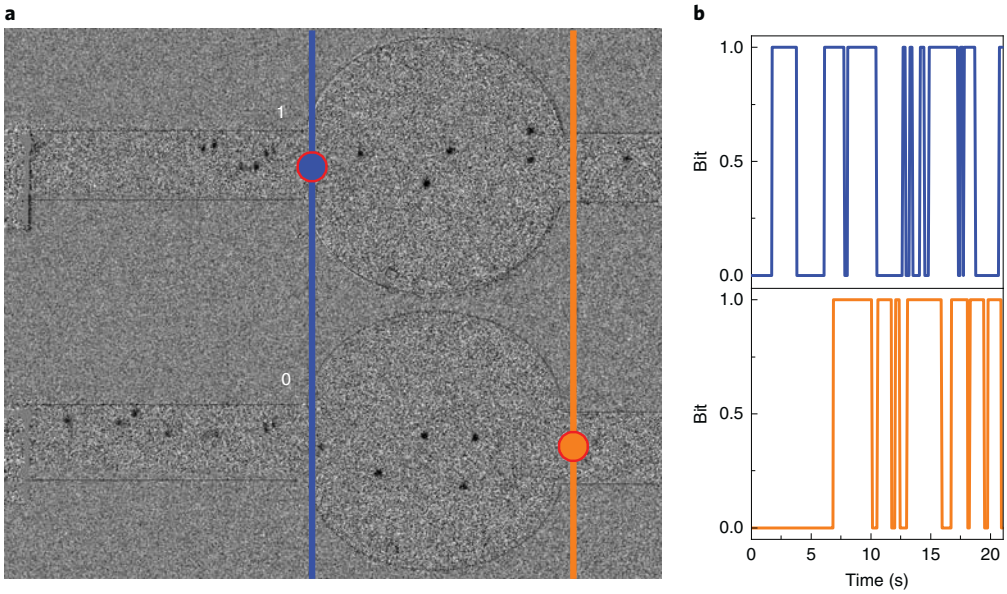

Fig. 3 | Observation of the skyrmion reshuffler device operation. a, Reshuffler operation with skyrmion nucleation by a direct current. The input signal is constructed as a time frame in which the skyrmion crosses the blue threshold line. The output is produced on crossing the orange line. **b**, The corresponding input signal is depicted in blue (top) and the resulting output signal in orange (bottom). The full process of the reshuffler operation is shown in Supplementary Video 5. The radius of the reshuffling chamber is 40 µm. The reconstructed p value for the input signal is $p_{\mathrm{input}} = 0.51 \pm 0.08$.

separate skyrmion streams and considered them as an example of an appropriately sampled input signal. Skyrmions were nucleated at the contact and then driven through the reshuffling chambers by applying a direct current (d.c.). The thermal diffusion led to a reshuffling of the order in which skyrmions enter and/or leave the system, thus decorrelating the output and input signals. To assess the functionality of the device, we compared the p values of the input and output to determine the fidelity. The deterministic generation of skyrmions as a result of input signal sampling was engineered to be an unrelated process not relevant to the reshuffling that we probed. The operation was recorded and evaluated as shown in Fig. 3. A real-time movie of the skyrmion reshuffler operation and the signal evaluation is shown in Supplementary Video 5. The p values of the in/output signals were calculated according to their definition, whereas the correlation of the two signals was evaluated using the equation for the Pearson correlation factor ρ:

$$\rho = \frac{\mathrm{cov}(\mathrm{in},\mathrm{out})}{\sigma_{\mathrm{in}}\sigma_{\mathrm{out}}} \qquad (2)$$

where cov is the covariance of the signals and σ is the s.d. of the respective signals. Evaluating the skyrmion reshuffler operation using a current density of $j = 3 \times 10^8\ \mathrm{A\,m^{-2}}$ in the wire that led to the reshuffling chamber and taking several operation runs into account, we obtained $p_{\mathrm{input}} = 0.51 \pm 0.08$. We found a negligible change of the p value between the input and output signals, $\Delta p = 0.01 \pm 0.08$, which shows the high fidelity of the signal retention. The calculated correlation factor was $\rho = 0.11 \pm 0.14$, which denotes the generation of an output signal that is highly uncorrelated to the device input signal. The total number of skyrmions used to represent and reshuffle the in/output signals was ~100, limited by the slow optical detection process used here. Larger numbers of skyrmion streams that exhibit faster diffusion, as is likely to be used in a real device in which electronic read-out times can be orders of magnitude faster than those using our optical technique, will lead to better statistics and even higher p value fidelities[13].

Our findings provide a number of statistical mechanics analysis methods for skyrmions: for example, the thermal dynamics can be used to quantify the energy landscape of a system and to determine the activation energy. Our results also introduce further possibilities to investigate the effects of soft-matter physics on skyrmion systems in thin films, for example, creep theorems and melting in two dimensions. The proof-of-concept reshuffler device demonstrates that the observed thermal skyrmion motion results in the creation of a signal highly uncorrelated to the device input while maintaining the same p value as the telegraph signal, which reveals the possibility of implementing skyrmion-based devices in probabilistic computing.

References

1. Jonietz, F. et al. Spin transfer torques in MnSi at ultralow current densities. *Science* **330**, 1648–1651 (2010).
2. Yu, X. Z. et al. Skyrmion flow near room temperature in an ultralow current density. *Nat. Commun.* **3**, 988 (2012).
3. Jiang, W. J. et al. Blowing magnetic skyrmion bubbles. *Science* **349**, 283–286 (2015).
4. Woo, S. et al. Observation of room-temperature magnetic skyrmions and their current-driven dynamics in ultrathin metallic ferromagnets. *Nat. Mater.* **15**, 501–506 (2016).
5. Litzius, K. et al. Skyrmion Hall effect revealed by direct time-resolved X-ray microscopy. *Nat. Phys.* **13**, 170–175 (2017).
6. Fert, A., Cros, V. & Sampaio, J. Skyrmions on the track. *Nat. Nanotechnol.* **8**, 152–156 (2013).

7. Zhang, X. et al. Skyrmion–skyrmion and skyrmion–edge repulsions in skyrmion-based racetrack memory. *Sci. Rep.* **5**, 7643 (2015).
8. Lin, S.-Z., Reichhardt, C., Batista, C. D. & Saxena, A. Particle model for skyrmions in metallic chiral magnets: dynamics, pinning, and creep. *Phys. Rev. B* **87**, 214419 (2013).
9. Reichhardt, C. & Reichhardt, C. J. O. Thermal creep and the skyrmion Hall angle in driven skyrmion crystals. *J. Phys. Condens. Matter* **31**, 07LT01 (2019).
10. Troncoso, R. E. & Núñez, Á. S. Brownian motion of massive skyrmions in magnetic thin films. *Ann. Phys. (N. Y.)* **351**, 850–856 (2014).
11. Xing, X., Pong, P. W. T. & Zhou, Y. Skyrmion domain wall collision and domain wall-gated skyrmion logic. *Phys. Rev. B* **94**, 1–11 (2016).
12. Huang, Y., Kang, W., Zhang, X., Zhou, Y. & Zhao, W. Magnetic skyrmion-based synaptic devices. *Nanotechnology* **28**, 08LT02 (2017).
13. Pinna, D. et al. Skyrmion gas manipulation for probabilistic computing. *Phys. Rev. Appl.* **9**, 064018 (2017).
14. Rózsa, L. et al. Skyrmions with attractive interactions in an ultrathin magnetic film. *Phys. Rev. Lett.* **117**, 157205 (2016).
15. Díaz, S. A., Reichhardt, C. J. O., Arovas, D. P., Saxena, A. & Reichhardt, C. Fluctuations and noise signatures of driven magnetic skyrmions. *Phys. Rev. B* **96**, 085106 (2017).
16. Schütte, C., Iwasaki, J., Rosch, A. & Nagaosa, N. Inertia, diffusion, and dynamics of a driven skyrmion. *Phys. Rev. B* **90**, 174434 (2014).
17. Miltat, J., Rohart, S. & Thiaville, A. Brownian motion of magnetic domain walls and skyrmions, and their diffusion constants. *Phys. Rev. B* **97**, 214426 (2018).
18. Mehrer, H. *Diffusion in Solids: Fundamentals, Methods, Materials, Diffusion-controlled Processes* (eds Cordona, M., Fulde, P., von Klitzing, K. & Queisser, H.-J.) (Solid State Sciences Vol. 155, Springer, 2007).
19. Nozaki, T. et al. Brownian motion of skyrmion bubbles and its control by voltage applications. *Appl. Phys. Lett.* **114**, 012402 (2019).
20. Gupta, P. K. & Kumaresan, R. Binary multiplication with PN sequences. *IEEE Trans. Acoust.* **36**, 603–606 (1988).

Acknowledgements

The project was funded by the Deutsche Forschungsgemeinschaft (DFG, German Research Foundation) project nos 403502522 and 49741853, SFB 767 and SFB TRR173, and grant no. EV 196/2-1. M.K., S.J. and G.J. acknowledge support from the WALL project (FP7-PEOPLE-2013-ITN 608031). L.R. acknowledges the support of the Alexander von Humboldt Foundation. P.V. thanks the DFG TRR146 for partial financial support. J.Z. acknowledges the help and advice of the technicians of the Kläui group, especially S. Kauschke.

Author contribution

M.K. and U.N. proposed and supervised the study. J.Z., S.J. and K.L. fabricated devices and characterized the multilayer samples. J.Z. and D.H. prepared the measurement set-up and, together with N.K. and S.K., conducted the experiments using the Kerr microscope. J.Z. and D.H. evaluated the experimental data with the help of P.V. and G.J. F.J. and A.D. performed the theoretical calculations and atomistic simulations of skyrmion diffusion. L.R. calculated the model parameters. J.Z. produced, measured and analysed the skyrmion reshuffler under the supervision of D.P., K.E.-S. and M.K. J.Z. drafted the manuscript with the help of M.K. and U.N. All the authors commented on the manuscript.

Competing interests

The authors declare no competing interests.

Methods

Sample parameters. The samples used in this study were grown as a continuous single layer stack of Ta(5)/$Co_{20}Fe_{60}B_{20}$(1)/Ta(0.08)/MgO(2)/Ta(5) (nanometre thickness of the layers shown in parenthesis). The sample was prepared by sputtering using a Singulus Rotaris sputtering tool with a base pressure of 3×10^{-8} mbar. Using a Singulus Rotaris deposition system, we can tune the thickness of the layers with a high accuracy (reproducibility better than 0.01 nm). The stack was annealed at 200 °C under vacuum for 1 h to optimize the properties, including the perpendicular magnetic anisotropy. It has been shown that introducing a very thin metal interlayer between the CoFeB and MgO layers can tune the perpendicular magnetic anisotropy of the material and result in a skyrmion phase nucleation at room temperature[21]. By tuning the layer thicknesses and optimizing the sputter parameters, we obtained films that exhibited skyrmions with thermal motion at room temperature and, by applying small out-of-plane external fields, the skyrmion size was adjusted. The hysteresis loop of the used sample shows a typical hour-glass shape, usually related to the presence of a magnetic skyrmion or stripe phase[4,22]. We found that at zero magnetic field a stripe domain phase was present in the material. Within the resolution of the measurement, the ratio between the two magnetization states (up and down sweeps) was within the measurement precision 1:1, which shows that the coercivity of the material was less than 0.05 mT. The threshold for the creation of a skyrmion was at 0.25 mT, which forms skyrmions with a radius of around 1 µm. Samples were then patterned by electron beam lithography into $60\times120\,\mu m^2$ pads with gold contacts for current injection. The sample was characterized with a superconducting quantum interference device and MOKE to determine the magnetic properties of the material stack.

The anisotropy field value was determined with a hard axis loop measurement using a superconducting quantum interference device[23]. The Dzyaloshinskii–Moriya interaction (DMI) of a multistack material can be calculated from the domain pattern periodicity based on the measured values for anisotropy and saturation magnetization[4,24]. We measured the worm domain periodicity around zero field and calculated the DMI using the obtained data assuming an exchange stiffness[25] of $A=10\,pJ\,m^{-1}$ and the thickness of the magnetic material of 1 nm. The domain periodicity was evaluated using a fast Fourier transformation (FFT) of the MOKE pictures obtained at zero field. The material parameters at 300 K are summed up in Supplementary Table 2.

Measurement set-up. The measurement set-up used was a commercial Evico GmbH MOKE microscope. The electromagnetic coil to supply the out-of-plane field was custom made at the University in Mainz and contains a Peltier element QC-32-0.6-1.2 to change the temperature of the studied sample while in ambient air. The achievable temperature range was 280–350 K. The temperature was controlled by resistivity measurement on a Pt100 resistor, which was placed on top of the Peltier element next to the sample. The stability of the set temperature was found to be within 0.3 K. The coil to induce the in-plane field was obtained from the microscope supplier. The microscope camera was capable of recording 16 frames per second, and therefore the timestep in the observation and evaluation of the skyrmion diffusion is 62.5 ms. Pulses for the current driven displacement were supplied by an Agilent 33250A Arbitrary Waveform Generator.

Current-induced dynamics. By current injection, we can nucleate single skyrmions in a deterministic fashion, and thereby control the density of the skyrmions precisely to avoid skyrmion–skyrmion interactions[14]. We first studied the skyrmions present for a fixed perpendicular field value of 0.35 mT, which led to a skyrmion radius of ~0.9 µm. To understand their topology, we analysed displacements driven by spin–orbit torque. The sample was subjected to 4 V for 5 ms to give a 96% probability of nucleating one skyrmion from the contact pad (Supplementary Video 1). Even for multiple pulse bursts, one pulse generated one new skyrmion in the sample when a 4 V bias was applied. Different origins of the nucleation have been discussed, such as heating and spin-torque effects in conjunction with local defects[26–29]. Our results indicate that a gradient in the current at the injection spot leads to skyrmion nucleation probably from a combination of heating and spin torques. As skyrmions are always nucleated at a certain location, we conclude the presence of a hotspot that at acts as a nucleation site for the skyrmions during current injection. Such a hotspot is preferential as it allows for reproducible skyrmion injection along defined paths.

On biasing with a current pulse, skyrmions already present in the sample moved synchronously in a direction opposite to the current direction in line with the DMI and spin Hall angle expected for a Ta-based stack[30]. The skyrmion velocity increased with current density, and for $6.4\times10^{10}\,A\,m^{-2}$ we obtained a velocity of $v=5\,mm\,s^{-1}$, similar to that reported previously[3]. As presented by Jiang et al.[3] on a stack with a similar composition, we can distinguish between chiral $Q=1$ skyrmions and non-chiral $Q=0$ magnetic bubbles by applying current. Non-chiral structures either expand or shrink in size on current injection, whereas chiral skyrmions move parallel to the current direction. That skyrmions move as a whole due to current indicates that the skyrmions have a topological charge $Q=1$, which also shows that they have the appropriate spin structure that exhibits an isotropic lateral diffusion that is optimal for the performance of the reshuffler. The velocity values differ from the values reported previously in Pt-based samples[5]. However, the investigated material stack has a reliable skyrmion nucleation and transport with current pulsing. At lower current densities (up to $6.4\times10^{10}\,A\,m^{-2}$), we also found the skyrmion Hall angle to be relatively constant at around 0°, as previously identified for low velocities[31].

Skyrmion imaging and tracking. We can use different approaches to nucleate skyrmions. The specific mechanism chosen for skyrmion generation is not crucial for our measurements, but we needed to have a sufficiently low skyrmion density to prevent significant skyrmion–skyrmion interaction during the diffusion. Although in our sample skyrmions can, for instance, be nucleated by external field sweeps, this procedure does not allow the skyrmion density to be easily controlled. Good control of the skyrmion density in our case was achieved by nucleating skyrmions at the electric contacts by injecting electric current pulses. This approach allowed us to fill the structure with skyrmions and, due to their repulsive interaction, we found a rather homogeneous skyrmion density. The diffusion measurements were, however, carried out with a lower skyrmion density to avoid skyrmion–skyrmion interaction (Supplementary Video 2).

Finding skyrmions and the determination of the skyrmion radius was done using a custom Wolfram Mathematica script. The program binarizes the frame with observed skyrmions and finds structures with one direction of magnetization. The binarization threshold is obtained by comparing the FFT of the original picture with the binarized picture using various thresholds. The threshold that yields the same FFT of the binarized picture as the FFT of the original one is then taken for further evaluation.

The spatial resolution of our MOKE microscope limited the determination of the magnetic structure profile, as the domain wall width of the skyrmion fell into less than one pixel of the measurement camera. Therefore, we saw a rapid intensity change within one pixel. All the observed skyrmions had a round shape with some deformations that fall into the resolution limit of the measurement technique. To determine the skyrmion radius, we fit the structures using the function 'EquivalentDiskRadius' in Wolfram Mathematica, which fits a disk that covers the same area as the observed structures. The errors of the skyrmion radius determination were then largely determined by the resolution of the microscope.

To track the skyrmion motion, the original images were evaluated instead of the binarized ones. We tracked the skyrmion motion with a 62.5 ms time resolution using the ImageJ[32] software with the TrackMate plugin[33,34] (Supplementary Video 3). The identification of skyrmions is based on their contrast and intensity and the validity of the tracking algorithm was confirmed by manual analysis and comparison over several samples. To apply the diffusion theory and obtain a reliable diffusion coefficient, we averaged over the measurement of several skyrmions.

To make use of the full statistics, the time-averaged MSD[35] was employed in the MSD evaluation using the data of all the skyrmions observed. In this method, the skyrmion position at every timeframe was used as a reference point (starting point) for that particular skyrmion tracking. The obtained MSDs for every starting point were then averaged over the whole time of the measurement video. This effectively means that there are many data points for shorter time differences, with only a few data points for longer timescales. Therefore, the statistical error largely increases with longer measurement times. To compensate for this, we only considered the timescales of half of the measurement time for the evaluation of the diffusion coefficient. The diffusion coefficient was obtained as a linear fit of the average MSD depending on time, as described in equation (1). The error of the evaluation was calculated as the s.d. of the MSDs of the observed skyrmions.

For the observation of skyrmion dwell times at different locations and to deduce the effect of the non-flat potential landscape, the time-averaged MSD was not used in the evaluation. Here only the skyrmion positions in the first frame of the observation video were taken as the reference for the calculation of the MSD and the evaluation of the dwell times.

The lowest temperature that we can analyse for this sample stack is about 290 K owing to the limitation of the total measurement time and the necessary displacement distances to obtain sufficient statistics for the case of low diffusion. Note that the temperature range is limited by the measurements in an ambient atmosphere, and above 305 K more and more skyrmions are nucleated, which leads to a skyrmion lattice formation, whereupon the assumption of non-interacting skyrmions breaks down.

For the reshuffler measurement, the current density is set as $j=3\times10^{8}\,A\,m^{-2}$, calculated at the moving pad before the reshuffling chamber. The current density inside the chamber was up to a factor of 4 lower due to the larger dimensions, which enhances the competition of skyrmion diffusion to current-induced motion. The dependence of the interplay between diffusion and current-induced displacement for different current densities is beyond the scope of this work, but was investigated theoretically[13]. The tracking of skyrmions was used to reconstruct the signal in the reshuffler operation. To evaluate the operation, we generated two separate skyrmion streams and assumed they were the result of an appropriately sampled input signal. By continuously generating skyrmions at the contact by direct current and driving them through the reshuffler chamber, we measured the input and output streams by detecting each skyrmion that crossed the blue and orange threshold lines (Fig. 3). On crossing the blue threshold line in front of the reshuffling chambers, the corresponding bit information (0 or 1, depending on which chamber the skyrmion enters) was triggered, which allowed

the reconstruction of the equivalent input signal that would have generated this specific sequence of skyrmions. The output signal was obtained using the same principle, where the order of the skyrmion crossing the orange threshold line allows for the reconstruction of an output telegraph signal (depicted in Fig. 3).

References

21. Yu, G. et al. Room-temperature creation and spin–orbit torque manipulation of skyrmions in thin films with engineered asymmetry. *Nano Lett.* **16**, 1981–1988 (2016).
22. Soumyanarayanan, A. et al. Tunable room-temperature magnetic skyrmions in Ir/Fe/Co/Pt multilayers. *Nat. Mater.* **16**, 898–904 (2017).
23. Büttner, F. et al. Magnetic states in low-pinning high-anisotropy material nanostructures suitable for dynamic imaging. *Phys. Rev. B* **87**, 134422 (2013).
24. Jaiswal, S. et al. Investigation of the Dzyaloshinskii–Moriya interaction and room temperature skyrmions in W/CoFeB/MgO thin films and microwires. *Appl. Phys. Lett.* **111**, 022409 (2017).
25. Lemesh, I., Büttner, F. & Beach, G. S. D. Accurate model of the stripe domain phase of perpendicularly magnetized multilayers. *Phys. Rev. B* **95**, 174423 (2017).
26. Sitte, M. et al. Current-driven periodic domain wall creation in ferromagnetic nanowires. *Phys. Rev. B* **94**, 064422 (2016).
27. Stier, M., Häusler, W., Posske, T., Gurski, G. & Thorwart, M. Skyrmion–anti-skyrmion pair creation by in-plane currents. *Phys. Rev. Lett.* **118**, 267203 (2017).
28. Büttner, F. et al. Field-free deterministic ultrafast creation of magnetic skyrmions by spin–orbit torques. *Nat. Nanotechnol.* **12**, 1040–1044 (2017).
29. Everschor-Sitte, K., Sitte, M., Valet, T., Abanov, A. & Sinova, J. Skyrmion production on demand by homogeneous DC currents. *New J. Phys.* **19**, 092001 (2017).
30. Lo Conte, R. et al. Role of B diffusion in the interfacial Dzyaloshinskii–Moriya interaction in Ta/$Co_{20}Fe_{60}B_{20}$/MgO nanowires. *Phys. Rev. B* **91**, 014433 (2015).
31. Jiang, W. et al. Direct observation of the skyrmion Hall effect. *Nat. Phys.* **13**, 162–169 (2017).
32. Schindelin, J. et al. Fiji: an open-source platform for biological-image analysis. *Nat. Methods* **9**, 676–682 (2012).
33. Jaqaman, K. et al. Robust single-particle tracking in live-cell time-lapse sequences. *Nat. Methods* **5**, 695–702 (2008).
34. Tinevez, J. Y. et al. TrackMate: an open and extensible platform for single-particle tracking. *Methods* **115**, 80–90 (2017).
35. Tejedor, V. et al. Quantitative analysis of single particle trajectories: mean maximal excursion method. *Biophys. J.* **98**, 1364–1372 (2010).